Constraints on Non-Standard Recombination from Recent CMB Observations

Angela M. Linn
*Department of Physics, The Ohio State University, Columbus, OH 43210**

Robert J. Scherrer
Department of Physics and Astronomy, Vanderbilt University, Nashville, TN 37235†

We examine cosmic microwave background constraints on variations in the recombination history of the universe. We use a very general extension to the standard model of recombination characterized by two parameters, a and b, which multiply the overall rates of recombination and ionization and the binding energies of hydrogen respectively. We utilize WMAP temperature and TE cross-correlation data, along with temperature data at smaller scales from ACBAR and CBI, to place constraints on these parameters. The range of recombination histories which gives the best fit to the data is $-0.6 < \log(a) < 0.5$ and $0.85 < b < 1.15$, forming a diagonal region from low-a/high-b to high-a/low-b. We find $z_{rec} = 1055 \pm 25$ and $\Delta z = 198 \pm 5$ at 68% confidence for the range of recombination models which are best able to reproduce the observed CMB power spectra. Standard recombination provides an acceptable fit to the data; while there is still room for non-standard recombination, the allowed variation is small.

I. INTRODUCTION

The cosmic microwave background (CMB) provides a snapshot of the early universe. The CMB radiation last interacted directly (i.e., non-gravitationally) with matter during the epoch of recombination, the period when the universe became cool enough for atomic nuclei to capture and hold electrons for the first time. Therefore, the CMB provides a sensitive test to any variations in the standard model of recombination.

A number of authors have looked at CMB constraints on variations in standard recombination [1, 2, 3, 4]. Here we reexamine this question in the light of recent, high-quality data from the WMAP satellite [5], ACBAR [6], and CBI [7], following the parametrization presented in Ref. [8]. The WMAP data represents a significant improvement over data used in most previous calculations, and significantly tightens the resulting constraints. In addition, we include the analysis of polarization data in the search for constraints on recombination. The only previous analysis to use the recent WMAP data has been given by Bean, et al. [4], who examined changes in the ionization history induced by Lyman-α photons and ionizing photons. Our approach is somewhat different; we have attempted a more general, model-independent investigation, based on the discussion in Ref. [8]. Hence, the constraints we derive are not tied to any particular model for altering recombination, but are potentially more general. Further, we have used additional data from ACBAR and CBI. In addition to using the TE cross-correlation data, we investigate the ability of the E-mode polarization power spectrum to further constrain recombination.

In Section II we describe a parameterization of the epoch of recombination and the details of how we obtain constraints on the parameters. In Section III we display the resulting constraints on recombination and discuss how the polarization power spectrum is affected by recombination. In Section IV we present our conclusions.

II. METHODS

A. Recombination Model

The ionization fraction x_e is the fraction of ionized hydrogen present in the universe,

$$x_e = n_e/n, \tag{1}$$

where n_e is the number density of free electrons and n is the number density of all hydrogen atoms, both ionized and neutral. The evolution of x_e is given by the ionization equation and describes the progress of recombination. The evolution of x_e is given by [9]

$$-\frac{dx_e}{dt} = C\left[Rn_p x_e^2 - \beta(1-x_e)\exp\left(-\frac{B_1 - B_2}{kT}\right)\right]. \tag{2}$$

Here C is Peebles' correction factor, R is the recombination coefficient, β is the ionization coefficient, B_1 and B_2 are the binding energies if the first two levels of hydrogen, and n_p is the number density of free protons plus hydrogen atoms.

It is our goal to constrain recombination in a general way, rather than investigating specific mechanisms. To that end, we follow the framework presented in Ref. [8] for modeling a general change in the evolution of the ionization fraction as a function of time. We modify the ionization history by inserting two parameters, a and b, into Equation (2):

$$-\frac{dx_e}{dt} = aC_P\left[\alpha n x_e^2 - \beta(1-x_e)e^{-b(B_1-B_2)/k_BT}\right]. \tag{3}$$

*Electronic address: linn.24@osu.edu
†Electronic address: robert.scherrer@vanderbilt.edu

The constant a multiplies the overall rates of both recombination and ionization, while the constant b multiplies the binding energies of hydrogen. The values $a = 1$ (or $\log(a) = 0$) and $b = 1$ are the case of standard recombination. We neglect any corresponding change in helium recombination, as that effect is small and for most models helium recombination is finished by the time hydrogen recombination begins. Very roughly, a change in a alone will change the duration of recombination, while keeping the onset of recombination fixed, while altering b shifts the onset of recombination to earlier or later redshifts.

B. Data Sets and Priors

Our goal is to find a range of recombination histories — that is, regions in a-b parameter space — which are capable of predicting CMB power spectra compatible with the observed CMB power spectra. We create a grid in a-b, and for each point in this space, we allow a set of five cosmological parameters to vary, as well as the overall normalization of the power spectrum. The vector of free parameters that we vary is ϑ=$\{\Omega_m,\ \omega_b,\ h,\ n_s,\ \tau_{RI},\ Q\}$: the matter density relative to critical Ω_m, the baryon matter density $\omega_b \equiv \Omega_b h^2$, the Hubble parameter h (in units of 100 km sec^{-1} Mpc^{-1}), the spectral tilt n_s, the optical depth to the surface of last scattering τ_{RI}, and the overall normalization of the power spectrum Q.

We assume priors for several of these cosmological parameters. For the Hubble parameter, we impose the constraint $h = 0.72 \pm 0.08$, consistent with estimates obtained from the Hubble Space Telescope (HST) Key Project and observations of Type Ia supernovae (SNe Ia) [10, 11]. The baryon density is taken from BBN constraints [12]: $\omega_b \equiv \Omega_b h^2 = 0.020 \pm 0.002$. Our estimate for the total matter density comes from supernovae studies [13, 14] and x-ray observations of the gas mass fraction of relatively relaxed galaxies [15]. We combine these, using generous error bars, to get $\Omega_m = 0.29 \pm 0.10$. These are all taken to be Gaussian, with uncertainties at the 68% confidence level. For the spectral tilt n_s we impose a uniform prior of $0.7 < n_s < 1.3$. Values of n_s beyond this range are disallowed. The reason for this is that n_s is generally not well known; indeed, the best estimates for the value of n_s come from the CMB itself [16, 17, 18]. Thus we use generous bounds which are theoretically motivated. We do not include priors for the optical depth τ_{RI} or the overall normalization of the power spectra Q. We additionally restrict our models to a flat ΛCDM universe ($\Omega_{tot} = 1$) and adiabatic initial density perturbations.

We then use `CMBFAST` [19] to produce a CMB anisotropy spectrum from our model, as a function of a, b, and ϑ. For each point in a-b space we vary ϑ to minimize χ^2, giving the combination of free parameters which is best able to reproduce the observed CMB power spectra for a given a and b.

For our data we use a combined set consisting of the WMAP temperature [20] and TE cross-correlation [21] data, along with smaller scale temperature data from ACBAR [7] and CBI [6, 22]. We follow the lead of Ref. [23] in combining the WMAP temperature data with the higher ℓ data from ACBAR and CBI. A calibration uncertainty of 20% is assumed for ACBAR and 10% for CBI. Although ACBAR has a 3% beam width uncertainty, this effect is extremely small compared to the calibration uncertainty and we neglect it. We minimize χ^2 using the combination of temperature and TE power spectra.

III. RESULTS

A. Effects of Varying the Recombination History

Altering a or b from their standard values has a direct effect on how recombination proceeds. The easiest way to see this is by looking at the ionization fraction x_e as a function of time. The ionization fraction determines the optical depth, τ due to Thomson scattering,

$$\tau = -\int_0^z c\sigma_T n_e(z)(dt/dz)dz, \tag{4}$$

which in turn gives the visibility function, $g(z)$:

$$g(z) = e^{-\tau} d\tau/dz, \tag{5}$$

Figure 1 shows the ionization fraction versus redshift for a variety of recombination histories (a, b). In each case, the free parameters ϑ are fixed at the values $\{\Omega_m = 0.29,\ \omega_b = 0.020,\ h = 0.72,\ n_s = 1.0,\ \tau = 0.15\}$. As a increases, recombination has a longer duration, though it starts at about the same time. Beyond a certain limit, roughly $\log(a) = 1.5$, recombination proceeds as rapidly as possible, and increasing a has no further effect because in the limit of high a, recombination proceeds in equilibrium. As b increases, the primary effect is that the onset of recombination shifts to earlier epochs. A secondary effect is that the duration of recombination increases with increasing b.

The resulting visibility functions of the models used in Figure 1 are shown in Figure 2. As a decreases, the redshift of recombination, z_{rec}, moves to more recent times, and the width Δz of the last scattering surface (LSS) increases. (We define z_{rec} to be the redshift at which the visibility function is peaked, while Δz is the full-width half-maximum of the visibility function). The degeneracy of models with sufficiently high values of a is clearly seen. As b decreases, the peak of the visibility function and z_{rec} move toward lower redshifts, just as with decreasing a. However, with decreasing b, unlike decreasing a, the width Δz decreases. Thus, at the expense of allowing Δz to change, changing a and b in opposite directions allows z_{rec} to remain relatively unchanged.

Changes to the recombination history have a direct effect on the temperature and polarization anisotropy spectra of the CMB. Decreasing a effectively increases the

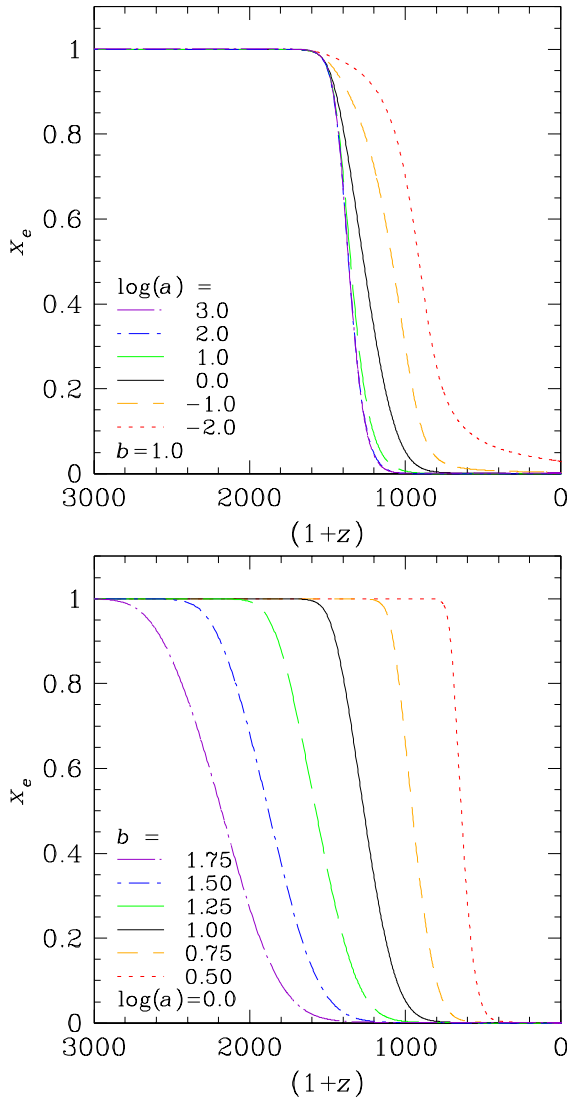

FIG. 1: The ionization fraction, $x_e(z)$, as a function of redshift, z, for varying a, fixed b (top) and for varying b, fixed a (bottom), for $\Omega_m = 0.29$, $\omega_b = 0.020$, $h = 0.72$, $n_s = 1.0$, $\tau_{RI} = 0.15$.

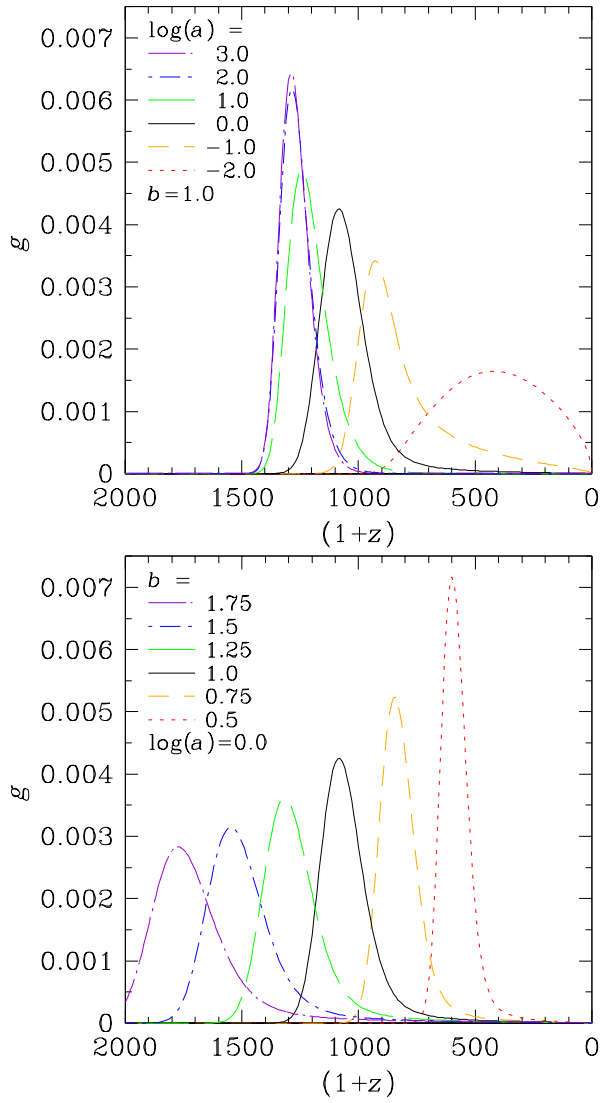

FIG. 2: As Fig. 1, for the visibility function $g(z)$.

width of the last scattering surface Δz, and to a lesser extent also decreases z_{rec}. The increase in Δz leads to increased diffusion damping of the anisotropies at large scales so that the peaks in the temperature, polarization, and TE cross-correlation power spectra at large scales are all less pronounced. The decrease in z_{rec} shifts the features of all three power spectra to larger scales.

Decreasing b primarily decreases z_{rec} and also leads to a slight decrease in the value of Δz. The decrease in z_{rec} will again shift the features of the power spectra to larger scales. In this case the relative amplitudes of the peaks vary considerably, whereas when a is varied, the relative amplitudes remain fairly constant: as b is increased, the height of the even peaks relative to the odd peaks is also increased. This is due to the change in the ratio of ρ_b to ρ_γ caused by later recombination. Because Δz increases only slightly as b is increased, diffusion damping at small scales for higher values of b is less significant.

B. Allowed Region in a-b Space

The region in a-b parameter space which is consistant with the CMB observations is displayed in Figure 3. This is the main result of our paper. The single best fit value is $\log(a) = -0.2$, $b = 1.0$, and standard recombination lies well inside the 1σ region. The allowed region of a-b space is considerably reduced compared to constraints using pre-WMAP data [8]. The 3σ region extends only from $-0.8 < \log(a) < 1.2$ and $0.70 \lesssim b \lesssim 1.25$. The 1σ regions are $-0.6 < \log(a) \lesssim 0.5$ and $0.85 < b < 1.15$.

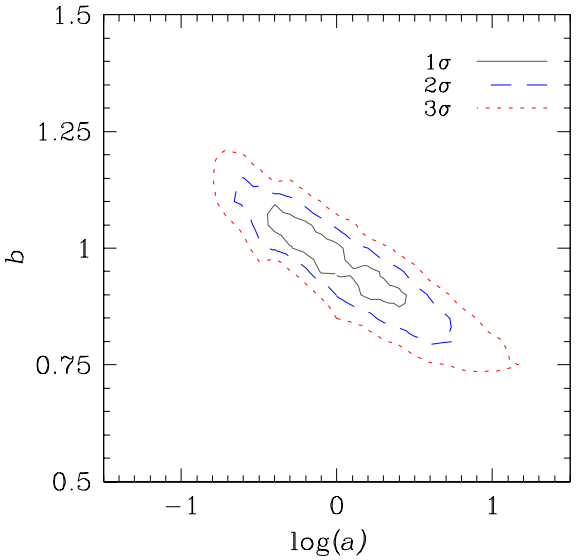

FIG. 3: Allowed region of a-b space. Solid, long-dashed, and short-dashed curves enclose the 1σ, 2σ, and 3σ regions.

C. Characteristics of the Allowed Regions

It is interesting to examine the manner in which the various cosmological parameters change in order to compensate for changes in a and b.

The shape of the CMB power spectrum is sensitive to changes in each of the cosmological parameters [24]. Increasing the baryon density suppresses the even peaks with respect to the odd peaks because the increased baryon mass contributes more gravity to the potential wells, lessening the effect of the rarefaction phase of the acoustic oscillations. Increasing the Hubble constant will lead to matter-radiation equality happening earlier and an increased expansion rate, thus the power spectrum will tend to have suppressed even peaks and move to slightly lower values of ℓ. An increase in the total matter density keeping the total density fixed at $\Omega_{tot} = 1$, or equivalently a decrease in the dark energy density, again moves matter-radiation equality to earlier times, which tends to move the spectra to lower ℓ and increase the late ISW effect. An increase in the scalar spectral index gives more power to smaller scales, and will tilt the CMB power spectrum, increasing the amplitude at large ℓ compared to small ℓ. Finally, increasing the optical depth due to reionization will decrease the power at small scales by a factor $e^{-2\tau_{RI}}$.

Figure 4 shows how the best-fit cosmological parameters change for all points falling inside the 3σ boundary. In producing this figure, we first determine the mean and 1σ variation for these parameters within the 1σ region in $a - b$ space. Then we calculate the best-fit value of each parameter for a given value of a and b. The open squares with $\times$'s show points for which the best-fit value for a given cosmological parameter lies within $\pm 1\sigma$ of the mean value. The solid squares show points for which the best-fit value of the given parameter is higher than this (i.e., more than 1σ above the mean), and the open squares show points for which the best-fit value is lower than 1σ below the mean.

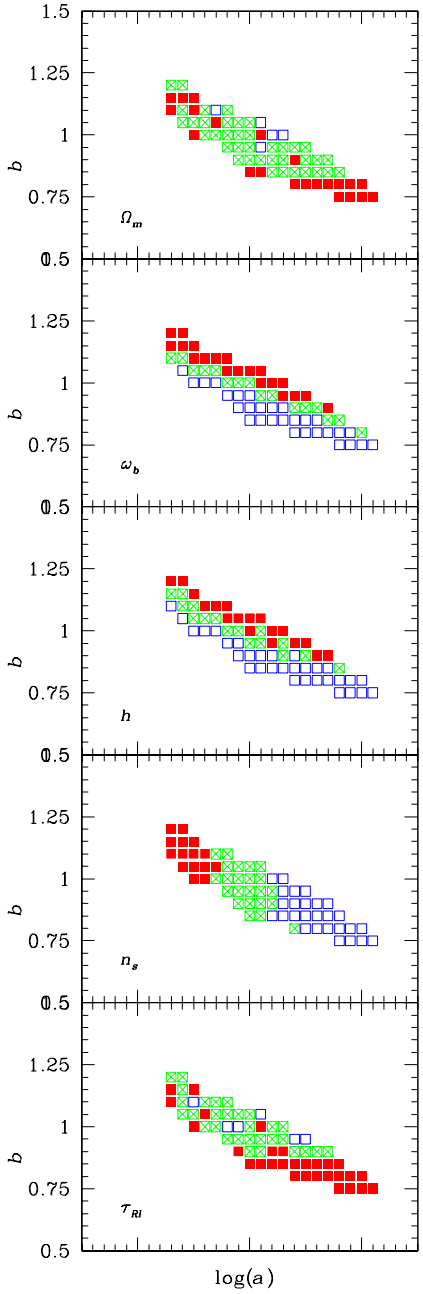

FIG. 4: How the best-fit cosmological parameters change with a and b for recombination histories falling inside the 3σ region. The squares with an $\times$ have "average" values for a given parameter, the solid squares have "high" values, and the open squares have "low" values. (See text for the precise definition).

The baryon density ω_b shows a strong tendency to increase both as a is increased and as b is increased. Similarly, the Hubble constant h increases both with increas-

ing a and increasing b. The scalar spectral index n_s increases with decreasing a but there does not appear to be any correlation of n_s with changing b. The optical depth τ_{RI} appears to increase with decreasing b, but this effect is not nearly so monotonic as the correlations in the previous three parameters. There does not appear to be any significant correlation of τ_{RI} with changes in a. For Ω_m, there does not appear to be much correlation with changes in a or b.

To summarize these effects, an increase in a is compensated by corresponding increases in ω_b and h and a corresponding decrease in n_s. An increase in b is compensated by increases in ω_b and h and possibly a decrease in τ_{RI}.

The corresponding changes in the cosmological parameters as a and b are changed are due to competing effects. As a is increased, the peaks at high ℓ are less damped, because the width of recombination is decreased, and the peaks are shifted to higher ℓ because recombination is moved to higher redshift. The decrease in n_s lowers the amplitude of the spectrum at small scales, counteracting the increased power at small scales due to a narrower surface of last scattering. An increase in h tends to move the peaks to larger scales, counteracting the effect of a higher z_{rec}. Similarly, increasing b will enhance the height of the even peaks by increasing z_{rec}, thus lowering the ratio of the baryon to photon density. This is compensated by a higher values of h and ω_b, which tend to suppress the height of the even peaks. The increased h will again move the peaks to slightly larger scales, even as an increase in b also increases z_{rec} and shifts the spectrum to smaller scales.

It is also instructive to look at the evolution of the ionization fraction x_e as a function of the redshift z for those recombination histories which provide a good fit to the data. Figure 5 shows x_e versus redshift for a selection of recombination histories in the 1σ, 2σ, and 3σ regions. In each case, the cosmological parameters used in calculating $x_e(z)$ were those which produced the best fit to the CMB data.

From Figure 5, it can be seen that the common feature in all recombination histories capable of producing the observed CMB is their ending point. The recombination histories start at different times and have different durations, but all end at approximately the same era. For the 1σ region, the average redshift at which the ionization fraction falls to 1% is $z(x_e = 0.01) = 856 \pm 20$. By contrast, the point where the ionization fraction falls to 50% has a much larger standard deviation: $z(x_e = 0.50) = 1237 \pm 44$. All error estimates are at the 68% confidence level.

We find a similar but smaller effect looking at the visibility function. Figure 5 shows the corresponding visibility functions $g(z)$ for the 1σ, 2σ and 3σ regions. For the 1σ region, we find that the average redshift of the peak of the visibility function is $z_{rec} = 1055 \pm 25$, while the average width is $\Delta z = 198 \pm 5$. If we look at the point where the visibility function falls to 10% of its peak value,

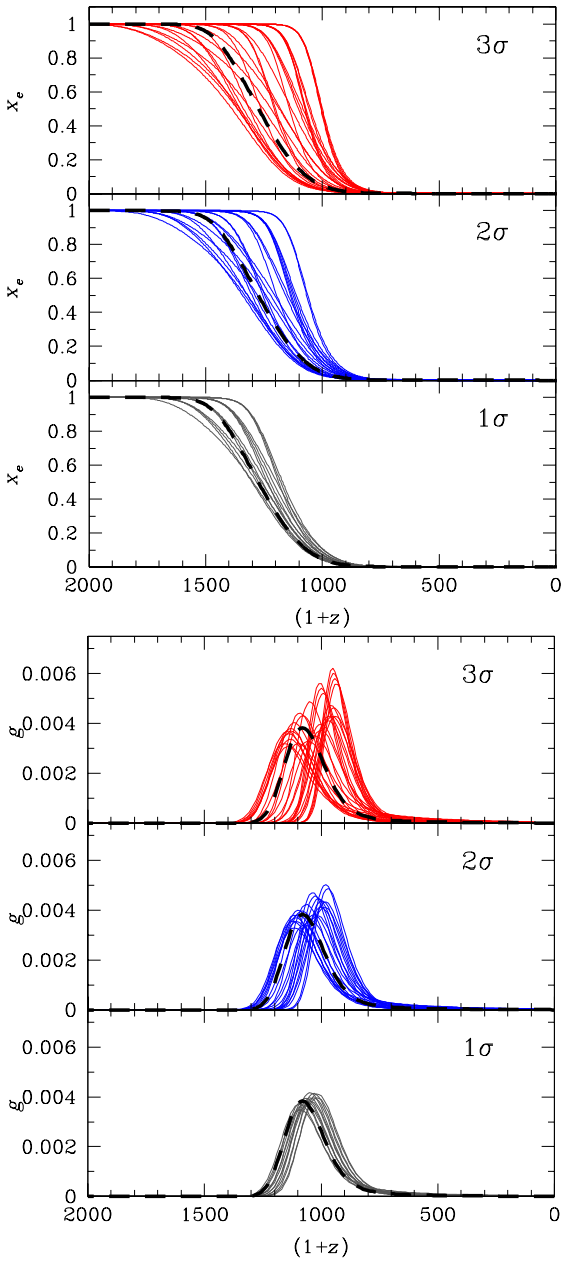

FIG. 5: Ionization fraction $x_e(z)$ vs. redshift z (top) and visibility function $g(z)$ vs. redshift z (bottom) for recombination histories falling within the 1σ, 2σ, and 3σ regions of the analysis. The thicker dashed line is standard recombination, and it falls within the 1σ region. It is shown on the other two graphs for comparison purposes.

we again find a somewhat tighter constraint than at the peak, $z(g/g_{max} = 0.10) = 811 \pm 19$, though the difference is not quite as great as that found using x_e.

The shapes of the visibility functions stray further and further from that of standard recombination in the 2σ and 3σ regions. Although some curves in the 3σ region have a similar z_{rec} to standard recombination, these curves tend to have a significantly different Δz. This suggests that we are not placing a constraint on z_{rec} or

Δz individually, but jointly.

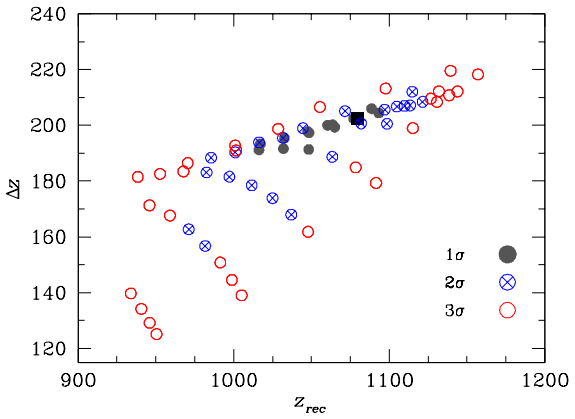

FIG. 6: Redshift of recombination z_{rec} vs. width of the last scattering surface Δz for recombination histories falling within the 1σ, 2σ, and 3σ regions of the WMAP+ TT+TE analysis. The apparent lines in this graph are due to the finite grid spacing in a and b.

In Figure 6, we have taken points from the 1σ, 2σ, and 3σ regions of the allowed a-b region, calculated their visibility functions, and plotted the resulting values of z_{rec} versus Δz. Although we are not drawing confidence regions in this $z_{rec} - \Delta z$ space, it can be clearly seen that the recombination histories which are best able to reproduce observations lie in a cluster, with successively poorer histories lying further out. As noted earlier, for all of the ionization histories inside the 1σ region, $z_{rec} = 1055 \pm 25$, and $\Delta z = 198 \pm 5$.

In Figure 7 we show the temperature, TE cross-correlation, and E-mode polarization power spectra for recombination histories falling within the 1σ region. The positions of the peaks in all three plots seem very well constrained, but the heights of the peaks differ somewhat. The $\mathcal{C}_\ell^{TT}$ and $\mathcal{C}_\ell^{TE}$ power spectra match the data very well, which is unsurprising since that was our criteria. Given the likely precision of data on the $\mathcal{C}_\ell^{EE}$ power spectrum in the near future, we conclude that it is unlikely that measurements of the E-mode polarization would be able to break any degeneracies in the allowed a-b parameter space and significantly improve the constraints on recombination.

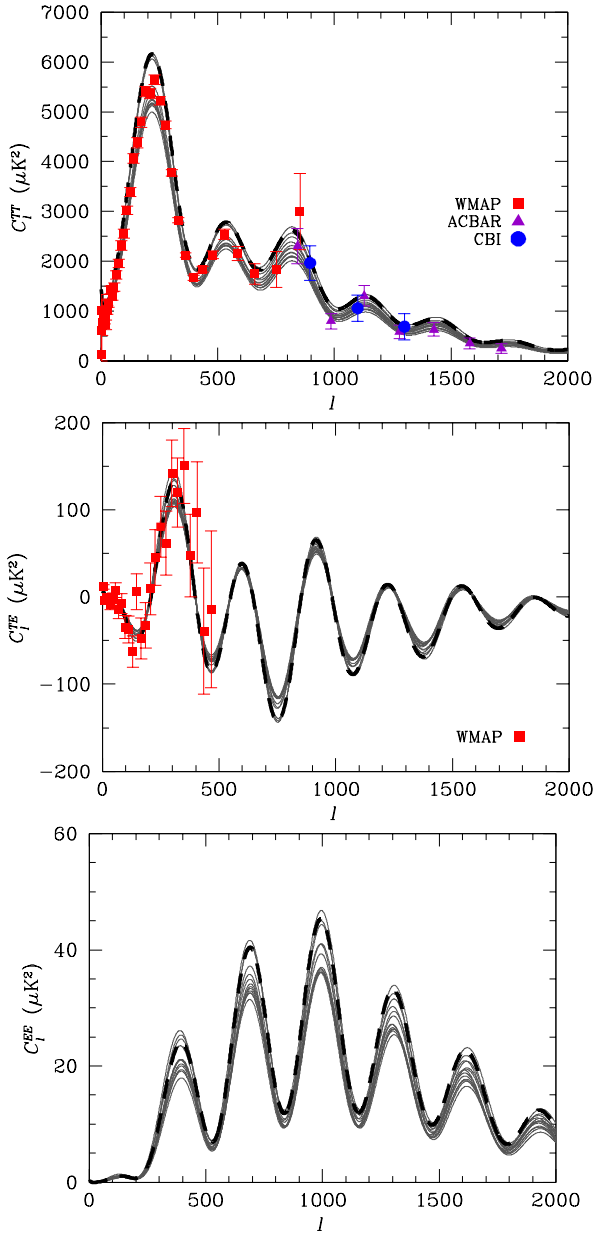

FIG. 7: $\mathcal{C}_\ell^{TT}$, $\mathcal{C}_\ell^{TE}$ and $\mathcal{C}_\ell^{EE}$ vs. ℓ for recombination histories falling inside the 1σ region. The thicker dashed line in each plot is standard recombination.

IV. CONCLUSIONS

We have examined the new data from the WMAP mission, along with data from higher ℓ experiments, ACBAR and CBI, in an attempt to constrain recombination. We have included analyses of both the temperature power spectrum $\mathcal{C}_\ell^{TT}$ and the TE cross-correlation power spectrum $\mathcal{C}_\ell^{TE}$. In the general parameterization that we used, the 1σ allowed region in a-b space was significantly contracted compared to earlier attempts with less precise data ([8]).

We find that the allowed region falls within $-0.6 < \log(a) < 0.5$ and $0.85 < b < 1.15$. The average width and position of the surface of last scattering for recombination histories falling within the 1σ region are $z_{rec} = 1055 \pm 25$ and $\Delta z = 198 \pm 5$. Note that the WMAP team estimated values for z_{rec} and Δz, namely [18] $z_{rec}^{\rm WMAP} = 1088^{+1}_{-2}$ and $\Delta z^{\rm WMAP} = 194 \pm 2$. Our values for z_{rec} and Δz do not mean the same thing as those reported by the WMAP team. In the latter case, standard recombination was assumed, and these values simply give the best-fit recombination history obtained by allowing the cosmological parameters to vary. In our case, we allow variations in

the recombination history itself, so we expect a larger range of values for z_{rec} and Δz. In fact, our values for z_{rec} and Δz are quite similar to the WMAP values; this is a reflection of the fact that standard recombination is an excellent fit to the data and is approximately in the center of the distribution of the allowed variant recombination histories.

The changes in a and b are largely compensated by changes in other parameters. The largest effects are that an increase in a is matched by corresponding increases in ω_b and h and a corresponding decrease in n_s, while an increase in b is compensated by increases in ω_b and h. Tighter constraints on these parameters, especially h, would allow us to narrow the range of allowed recombination histories.

The result of these competing effects — changes in a and b being partially compensated for by changes in the free cosmological parameters — is that the anisotropy power spectra from the 1σ region all share very similar features. In general, the positions of the peaks are strongly constrained, while the amplitudes of the peaks are less so. The range in E-mode polarization power spectra corresponding to recombination histories from this region is very similar to the range in temperature and TE cross-correlation power spectra, and is unlikely to be useful in breaking degeneracies in a-b parameter space.

We find that the range of alternate recombination histories allowed by the WMAP, ACBAR, and CBI temperature and WMAP TE cross-correlation data is very small compared to that allowed by earlier data, and is approximately centered on standard recombination. While there is still some room for non-standard recombination histories, the constraints have narrowed considerably with this new data. Standard recombination fits the data extremely well, and there is no compelling evidence from this study to suggest that a non-standard recombination is preferable.

V. ACKNOWLEDGMENTS

A.M.L. and R.J.S. were supported in part by the Department of Energy (DE-FG02-91ER40690) at Ohio State University.

[1] Peebles, P. J. E., Seager, S., & Hu, W. 2000, Astrophys. J., 539, L1
[2] Landau, S., Harari, D., & Zaldarriaga, M. 2001, Phys. Rev. D, 63, 3505
[3] Doroshkevich, A. G., & Naselsky, P. D. 2002, Phys. Rev., D65, 123517
[4] Bean, R., Melchiorri, A., & Silk, J. 2001, Phys. Rev., D68, 083501
[5] Bennett, C. L., et al. 2003, Astrophys. J. Suppl., 148, 1
[6] Pearson, T. J., et al. 2003, Astrophys. J., 591, 556
[7] Kuo, C.-l., et al. 2002
[8] Hannestad, S., & Scherrer, R. J. 2001, Phys. Rev., D63, 083001
[9] Peebles, P. J. E. 1968, Astrophys. J., 153, 1
[10] Freedman, W. L., et al. 2001, Astrophys. J., 553, 47
[11] Gibson, B. K., & Brook, C. B. 2000
[12] Steigman, G. 2002, Fortsch. Phys., 50, 562
[13] Perlmutter, S., et al. 1999, Astrophys. J., 517, 565
[14] Riess, A. G., et al. 1998, Astron. J., 116, 1009
[15] Allen, S. W., Schmidt, R. W., & Fabian, A. C. 2002, Mon. Not. Roy. Astron. Soc., 334, L11
[16] Benoit, A., et al. 2003, Astron. Astrophys., 399, L25
[17] Jaffe, A. H., et al. 2003, New Astron. Rev., 47, 727
[18] Spergel, D. N., et al. 2003, Astrophys. J. Suppl., 148, 175
[19] Seljak, U., & Zaldarriaga, M. 1996, Astrophys. J., 469, 437
[20] Hinshaw, G., et al. 2003, Astrophys. J. Suppl., 148, 135
[21] Kogut, A., et al. 2003, Astrophys. J. Suppl., 148, 161
[22] Mason, B. S., et al. 2003, Astrophys. J., 591, 540
[23] Verde, L., et al. 2003, Astrophys. J. Suppl., 148, 195
[24] Bersanelli, M., Maino, D., & Mennella, A. 2002, Riv. Nuovo Cim., 25, 1